



Search for WH associated production with 8.5 fb^{-1} of Tevatron data

The DØ Collaboration
URL <http://www-d0.fnal.gov>

Dated November 15, 2011

We present a search for WH production in $p\bar{p}$ collisions at a center of mass energy of $\sqrt{s} = 1.96 \text{ TeV}$ in data recorded by the DØ experiment corresponding to an integrated luminosity of 8.5 fb^{-1} . We apply a multivariate technique to events containing one lepton, an imbalance in transverse energy and one or two tagged b -jets to discriminate a potential WH signal from standard model backgrounds. We observe good agreement between data and expected background, and for $M_H = 115 \text{ GeV}$ we set an upper limit of 4.6 at 95% C.L. on the ratio of $\sigma(p\bar{p} \rightarrow WH) \times \mathcal{B}(H \rightarrow b\bar{b})$ to its standard model prediction while from simulation we expect a limit of 3.5 on the ratio. We also apply the multivariate technique trained with WZ and ZZ events as signal to study our sensitivity to $WZ + ZZ$ production. We measure a cross section of $7.20 \pm 2.03(\text{stat.}) \pm 2.74(\text{syst.}) \text{ pb}$, with a significance of 2.2 standard deviations. A significance of 1.4 is expected from simulation.

The only unobserved particle of the standard model (SM) is the Higgs boson, which emerges from the spontaneous breaking of electroweak symmetry. Its identification would confirm the hypothesis that the Higgs mechanism generates the masses of the weak gauge bosons, and also provides an explanation for the finite masses of fermions via their Yukawa couplings to the Higgs field. The mass of the Higgs boson (M_H) is not predicted in the SM, but the combination of results from direct searches at the CERN e^+e^- Collider (LEP) [1] and precision measurements of other electroweak parameters constrain M_H to $114.4 < M_H < 186$ GeV at 95% C.L [2]. While the M_H region 158–173 GeV is excluded at 95% C.L. by the CDF-D0 combined analysis [3], the remaining allowed mass range is being probed further at the Fermilab Tevatron Collider. The associated production of a Higgs boson and a W boson is among the cleaner Higgs channels at the Tevatron, and has the largest yield for the product of the cross section and branching fraction of $H \rightarrow b\bar{b}$ for $M_H < 125$ GeV. Several searches for WH production have already been published at a $p\bar{p}$ center-of-mass energy of $\sqrt{s} = 1.96$ TeV. Four of these [4–7] use subsamples (0.17 fb^{-1} , 0.44 fb^{-1} , 1.1 fb^{-1} and 5.3 fb^{-1}) of the data analyzed in this paper, while the most recent publication from the CDF collaboration is based on 2.7 fb^{-1} of integrated luminosity [8].

We present a new search using a multivariate approach in 8.5 fb^{-1} of total integrated luminosity collected by the D0 experiment. The search is based on events with one charged lepton ($\ell = e$ or μ), an imbalance in transverse energy (\cancel{E}_T) that arises from the neutrino in the $W \rightarrow \ell\nu$ decay, and either two or three jets, with one or two of these jets selected as a candidate b -quark jet (b -tagged). We also present a measurement of the $WZ + ZZ$ cross section in order to validate our Higgs search methods.

The channels are separated into orthogonal selections of events with exactly one b -tagged jet and with two b -tagged jets. Single b -tagged events contain three important sources of backgrounds: (i) multijet events, where a jet is misidentified as an isolated lepton, (ii) W boson production in association with c -quark or light-quark jets, and (iii) W boson production in association with two heavy-flavor ($b\bar{b}, c\bar{c}$) jets. In events with two b -tagged jets, the dominant backgrounds are from $Wb\bar{b}$, $t\bar{t}$, and single top-quark production. We use a Boosted Decision Tree (BDT) multivariate technique (MVA) to separate the SM background from signal in the selected events and search for an excess, expected primarily at large values of the MVA discriminant. A separate MVA discriminant is created for each combination of final state jet multiplicity (2 or 3), lepton flavor (e or μ), and number of b -tagged jets (1 or 2). Because of detector upgrades and algorithm improvements, we split our data into three epochs: Run IIa (2002- March 2006), Run IIb1 (June 2006 - August 2007) and Run IIb2 (August 2007 - March 2011). In total, we have 24 orthogonal subchannels. Here we describe only the analysis of the Run IIb1 + Run IIb2 data (collectively denoted “Run IIb”) totaling 7.5 fb^{-1} ; the Run IIa portion of the analysis (1.0 fb^{-1}) is unchanged from [7]. We consider all channels simultaneously when performing our search and final limit setting. For the $WZ + ZZ$ cross section measurement, we consider only the Run IIb dataset analyzed here.

The analysis relies on the following components of the D0 detector [9]: a central-tracking system, which consists of a silicon microstrip tracker (SMT) and a central fiber tracker (CFT) located within a 1.9 T superconducting solenoidal magnet; a liquid-argon/uranium calorimeter consisting of a central section (CC), covering pseudorapidity $|\eta| < 1.1$ relative to the center of the detector [10], and two end calorimeters (EC) extending coverage to $|\eta| < 4.2$, all housed in separate cryostats [11], with scintillators between the CC and EC cryostats providing additional sampling of developing showers at $1.1 < |\eta| < 1.4$; and a muon system located beyond the calorimetry which consists of layers of tracking detectors and scintillation trigger counters before and after the 1.8 T iron toroids. A 2006 detector upgrade added an additional layer of silicon to the SMT [12], an improved calorimeter trigger [13], and improved tracking electronics.

The luminosity is measured using plastic scintillator arrays located in front of the EC cryostats at $2.7 < |\eta| < 4.4$. We reject data in which the tracking (CFT and SMT), calorimeter or muon information may have been compromised. The trigger and data acquisition systems are designed to accommodate the high instantaneous luminosities of Run II.

Events in the electron channel are triggered by a logical OR of several triggers requiring an electromagnetic (EM) object and one jet. Trigger efficiencies are taken into account in the simulation through a reweighting of events, based on an efficiency derived from data, and parametrized as a function of electron η , azimuth ϕ , and jet p_T .

We accept muon channel events from an inclusive mixture of single muon, muon plus jet, \cancel{E}_T plus jet, and multijet triggers. To verify the efficiency of the inclusive set of triggers, we compare events that pass a well-modeled subset of single muon triggers to those that pass a complementary trigger from the inclusive set of triggers. Good agreement is observed between data and MC when using the single muon subset of triggers. We determine the efficiency of the complementary set of triggers in data and model it as a function of the scalar sum of jet p_T (H_T) and muon ϕ . This model provides an additive correction to the efficiency of the single muon triggers in our MC of $\approx 36\%$, and we observe good agreement between data and MC when combining the single muon and complementary triggers to form the inclusive trigger set.

Simulation of background and signal processes relies on the CTEQ6L1 [14] leading-order parton distribution functions for all MC event generators. The PYTHIA [15] MC generator is used for simulating the production of dibosons with inclusive decays (WW, WZ and ZZ), $WH \rightarrow \ell\nu b\bar{b}$ and $ZH \rightarrow \ell\bar{\ell} b\bar{b}$ ($\ell = e, \mu$, or τ). The $W(Z)$ +jets and $t\bar{t}$

events are generated with ALPGEN [16] interfaced to PYTHIA for parton showering and hadronization. ALPGEN samples are produced using the MLM parton-jet matching prescription [16]. The $W(Z)$ +jets samples contain $W(Z)jj$ and $W(Z)cj$ processes, while $W(Z)b\bar{b}$ and $W(Z)c\bar{c}$ are generated separately. Single top-quark events are generated using COMPHEP [17] and use PYTHIA for parton evolution and hadronization. All generated events are processed through a full D0 detector simulation (based on GEANT [18]), using the same reconstruction software as used for D0 data. Data events from random beam crossings are overlaid to account for multiple $p\bar{p}$ interactions. Simulated events are reweighted for differences in trigger efficiencies of MC simulations relative to data, which depend on the analysis channel, data epoch, and event kinematics.

The simulated background processes are normalized to the SM predictions for their cross sections, except for W/Z +jets events, which are normalized to data before applying b -tagging, where the contamination from signal is expected to be negligible. The signal cross sections are from [19], computed with the MSTW2008 PDF set [20]. The $t\bar{t}$, single-top, and diboson cross sections are at NLO (resummed NLO for $t\bar{t}$), and taken from Ref. [21], Ref. [22], and the MCFM program [23], respectively. As a cross check, we compare data with the ALPGEN prediction for W +jets, corrected in such a way that the inclusive W production cross section is equal to its NNLO calculation [24] with MRST2004 NNLO PDFs [25], and we find a relative data/MC normalization factor of 1.0 ± 0.1 for W +jets, where the normalization factor for data is obtained after subtracting all other expected background processes. For the W +heavy-flavor jet events, the phenomenological ratio of leading-order to NLO corrections for $Wb\bar{b}$ and W +light jets obtained from MCFM is consistent with experiment, so that we do not apply additional corrections, and the corresponding factors are also used for the Z +heavy-flavor jet processes.

This analysis is based on the selection of events with only one electron with $p_T > 15$ GeV and $|\eta| < 1.1$ or $1.5 < |\eta| < 2.5$, or only a single muon with $p_T > 15$ GeV and $|\eta| < 1.6$. Events are also required to have $\cancel{E}_T > 15(20)$ GeV for the electron (muon) channel, either exactly two or three jets with $p_T > 20$ GeV (after calibration of the jet energy [26]) and $|\eta| < 2.5$. \cancel{E}_T is calculated from the individual calorimeter cells, except for unclustered energy in cells of the outermost readout layers of the calorimeter, and is corrected for the presence of any muons. All energy corrections to electrons or to jets are propagated into \cancel{E}_T .

Events with additional charged leptons, isolated from jets, that pass a flavor-dependent p_T threshold ($p_T^e > 20$ GeV, $p_T^\mu > 15$ GeV and $p_T^\tau > 10$ or 15 GeV, depending on τ decay channel) are rejected to suppress dilepton background from Z and $t\bar{t}$ events. Only events with a primary vertex (with at least three tracks) located within ± 60 cm of the nominal longitudinal interaction point, measured along the beam axis, are selected for further analysis.

Leptons candidates are identified in two steps: (i) Each candidate must pass “loose” identification criteria, which for electrons requires 95% of the energy in a shower to be deposited in the EM section of the calorimeter, a calorimeter isolation fraction (ratio of the EM energy in a $\Delta\mathcal{R} < 0.2$ cone in the (η, ϕ) space [10] to the total calorimeter energy in a $\Delta\mathcal{R} < 0.4$ cone around the lepton) less than 0.1, requirements on the spatial distribution of EM showers, a reconstructed track matched to the EM shower, and isolation criteria for that matched track. For the loose muon, we require the timing of scintillator hits to coincide with beam crossings (to veto cosmic-rays), a match of the reconstructed track in the muon system with one in the central tracker, and isolation from jets to reject muons from semileptonic decay of hadrons ($\Delta\mathcal{R} > 0.5$). (ii) The loose leptons then undergo a final “tight” selection: tight electrons have to satisfy more restrictive calorimeter isolation fraction and EM energy proportion criteria (< 0.07 and $> 97\%$, respectively), and satisfy a likelihood test developed on $Z \rightarrow ee$ data based on eight quantities characterizing the EM nature of the particles [27]. Tight muons must satisfy stricter isolation criteria on energy in the calorimeter and momenta of tracks near the trajectory of the muon candidate. Inefficiencies introduced by lepton-identification and isolation criteria are determined from $Z \rightarrow \ell\ell$ data. The final selections rely only on tight leptons, with loose leptons used to determine the multijet background.

Instrumental backgrounds and those from semi-leptonic decays of hadrons, referred to jointly as the multijet background, are estimated from data. The instrumental background is important for the electron channel, where a jet with high EM fraction can pass electron-identification criteria, or a photon can be misidentified as an electron. In the muon channel, the multijet background is less important, and arises mainly from the semi-leptonic decay of heavy quarks, where the muon satisfies the isolation requirements.

To estimate the number of events containing a jet passing tight lepton selection, we determine the probability, $f_{T|L}$, for a loose-lepton candidate originating from a jet to also pass tight identification. This is done in events that pass preselection requirements, i.e., containing one loose lepton and two jets, but with small \cancel{E}_T (5 – 15 GeV). The total non-multijet background is estimated from MC and subtracted from the data before estimating the contribution from multijet events. The probability $f_{T|L}$ is defined by the ratio of the estimated multijet contribution including only tight leptons to that containing loose leptons (which also includes tight leptons). For electrons, $f_{T|L}$ is determined as a function of electron p_T in three regions of $|\eta|$ and four in $\Delta\phi(\cancel{E}_T, e)$, while for muons it is taken as a function of p_T for two regions of $|\eta|$ and eight regions of $\Delta\phi(\cancel{E}_T, \mu)$. The efficiency for a loose lepton to pass the tight identification ($\varepsilon_{T|L}$) is measured in $Z \rightarrow \ell\ell$ events in data, and is modeled as a function of p_T for both electrons and muons. A modified version of the “matrix” method [27] is used to determine the multijet background directly from data, where

each event is assigned a weight that contributes to the multijet estimation based on $f_{T|L}$ and $\varepsilon_{T|L}$ as a function of event kinematics. Since $f_{T|L}$ depends on \cancel{E}_T , the scale of this estimate of the multijet background must be adjusted when comparing to data with $\cancel{E}_T > 15(20)$ GeV for electron (muon) channels. Before applying b -tagging, we perform a fit to the transverse mass of the W candidate (M_W^T) distribution to set the scale of the pure multijet and W/Z +jets backgrounds simultaneously.

Jets are reconstructed using a midpoint cone algorithm [28] with a radius of $\Delta\mathcal{R}_y = \sqrt{(\Delta y)^2 + (\Delta\phi)^2} = 0.5$, where y is the jet rapidity. Identification requirements ensure that the distribution in jet energy for all layers of the calorimeter is reasonable and that jets are not caused by noise or spurious depositions of energy. The difference in efficiency for jet identification and jet resolution between data and simulation is taken into account in the overall MC correction for jet reconstruction efficiency and energy scale. Comparison of ALPGEN with other generators and with data show some discrepancies in distributions of jet pseudorapidity and dijet angular separations [29]. The data are therefore used to correct the ALPGEN W +jets and Z +jets MC events by reweighting the simulated η of the leading and second-leading jet, the $\Delta\mathcal{R}$ between the two leading jets, and the W p_T variables in the W/Z +jets samples through the use of polynomial functions that bring the total simulated background into agreement with the high statistics pre- b -tagged data. After this step, the jet distributions in simulations are in agreement with the data over the complete range of kinematics.

To suppress multijet background, events with $M_W^T < 40\text{GeV} - 0.5 \cancel{E}_T$ GeV are removed in the muon channel. In the electron channel, we develop a multivariate technique (MVAQCD) that exploits kinematic differences between the multijet background and signal. The MVAQCD is a Boosted Decision Tree (BDT) developed with the TMVA package [30]. It employs the variables listed in Table I as inputs. We train with a mixture of signal MC events from all considered Higgs masses as the signal, and with data events that pass the loose lepton selection but fail the tight selection as the background. We verify that the output distribution is well-modeled, and apply a loose cut on the output distribution. The cut has a 97% efficiency for signal while rejecting 75% of the multijet background.

TABLE I: Table of MVAQCD input variables.

| Variable | Definition |
|------------------------------|--|
| η_ν | The neutrino pseudorapidity, calculated by choosing the smaller absolute value of the 2 neutrino longitudinal momentum solutions, assuming the electron and \cancel{E}_T are the products of an on-shell W decay |
| \cancel{E}_{Tsig} | The missing- E_T significance: likelihood that the \cancel{E}_T arises from physical sources |
| $\Delta\eta(\nu, electron)$ | $\Delta\eta$ between the electron and neutrino (neutrino η calculated as above) |
| W twist | $\tan^{-1}\left(\frac{\Delta\phi(\nu, e)}{\Delta\eta(\nu, e)}\right)$ (neutrino η calculated as above) |
| $\cos\theta_\ell$ | Cosine of the lepton polar angle in the (e, ν) center of mass system |
| Σ_{min}^H | $\frac{\Delta R(j_1, j_2) \cdot p_T^{j, max}}{\sum p_T^j}$ where $p_T^{j, max}$ corresponds to the highest jet p_T |
| Higgs decay product velocity | $-\log\left(1 - \sqrt{1 - 4\sqrt{(m_1 + m_2)/m}}\right)$ where m_1 , m_2 , and m are respectively the leading, sub-leading and di-jet invariant mass |
| WH asymmetry | Mass asymmetry between W and H candidates: $(m_W - m_{bb})/(m_W + m_{bb})$ |

Efficient identification of b -jets is central to the search for WH production. The D0 b -tagging algorithm for identifying heavy-flavored jets is based on a combination of seven variables sensitive to the presence of tracks or secondary vertices displaced significantly from the primary vertex. It also makes use of Boosted Decision Trees and provides improved performance over the algorithm described in [31]. The efficiency is determined for taggable jets, i.e., jets with at least two tracks of good quality with at least one hit in the SMT. Simulated events are corrected to have the same fraction of jets satisfying the taggability and b -tagging requirements as found in preselected data. For jets that are not taggable, the b -tagging algorithm output is 0.

We choose a b -ID operating point that corresponds to an identification efficiency of $\approx 79\%$ for true b -jets, and to a misidentification rate of $\approx 11\%$ for “light” parton jets (u, d, s, g), both for jets of $p_T \approx 50$ GeV. We split our events into two samples: events with only one jet b -tagged (single tag or ST), and events with two b -tags (double tag or DT). This definition of two orthogonal samples, DT and ST, improves sensitivity to a potential signal beyond choosing a single b -tagging category.

After applying these selection criteria, the expected event yields for specific backgrounds and for a Higgs boson with $M_H = 115$ GeV are compared to the observed number of events in Table II. Distributions of the dijet invariant mass, using the two jets of highest b -ID output, in $W+2$ -jets and $W+3$ -jets events are shown for the ST and DT samples in Fig. 1(a-d). The data are well described by the sum of the simulated SM processes and multijet background. The contributions expected from a Higgs boson with $M_H = 115$ GeV are also shown.

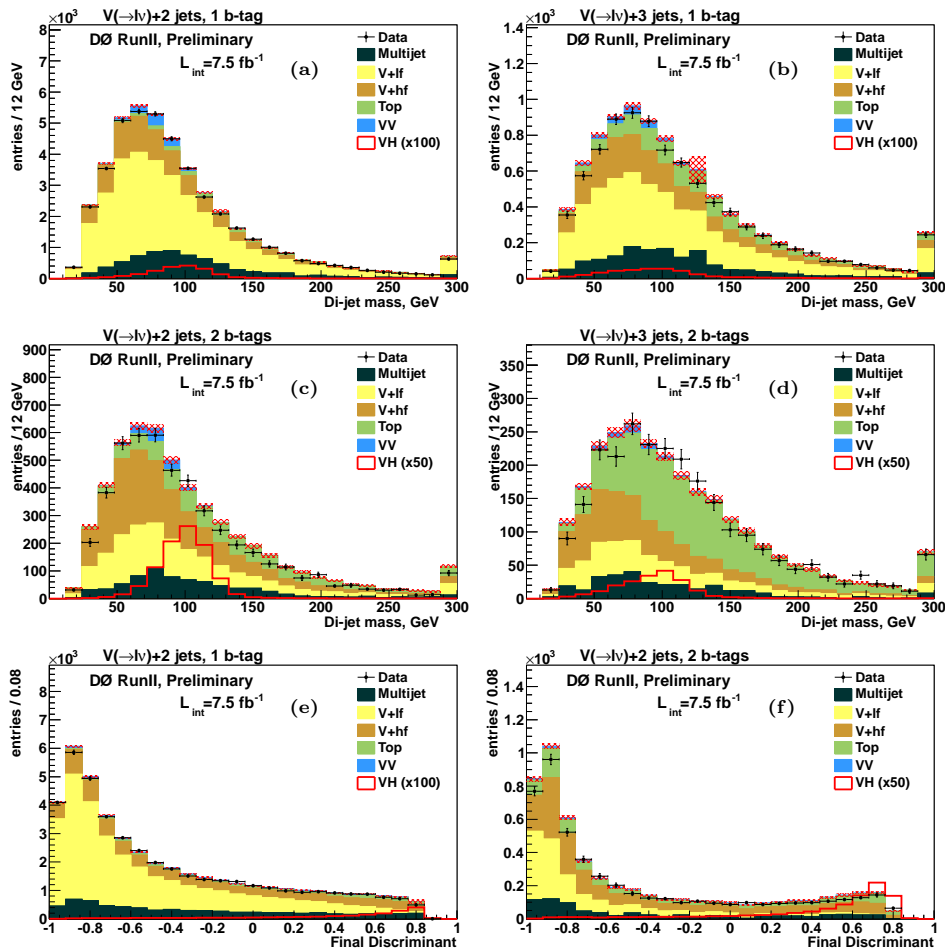


FIG. 1: Dijet mass distributions for the $W+2$ -jets, $W+3$ -jets ST events (a,b) and DT (c,d) events (e and μ channels are combined in all cases) in the Run IIB dataset. For 3-jet events we use the two jets with the highest b -ID output to form the dijet mass. The data are compared to the background prediction. The VV contribution is the sum of the WW , WZ , and ZZ samples. The distributions in the final MVA discriminant for $W+2$ -jet ST and DT events are shown in (e,f), respectively. The expected signal for $M_H = 115$ GeV is shown scaled by 100 (ST) or 50 (DT).

To further separate signal and background we apply a multivariate analysis technique (MVA) to the selected events. An MVA discriminant based on Boosted Decision Trees from the TMVA package uses the kinematic variables of Table III as inputs. When selecting input variables we ensure that each is well-modeled and displays good separation between signal and one or more backgrounds. We train a separate MVA for each Higgs mass considered, with M_H varying between 100–150 GeV in 5 GeV steps, for each of the 16 independent channels of the Run IIB1 and Run IIB2 datasets. All channels are considered simultaneously when performing our search and final limit setting. Figures 1(e,f) show the MVA output distribution in Run IIB data for 2-jet ST and DT events, respectively. In order to study our sensitivity to $WZ + ZZ$ production and to show that we can isolate known processes with small cross sections in the same final state as WH , we also train a discriminant with WZ and ZZ production as signal sources, using the same input variables in Table III.

The systematic uncertainties that affect the signal and SM backgrounds can be categorized by the nature of their source, i.e., theoretical (e.g., uncertainty on a cross section), MC modeling (e.g., re-weighting of ALPGEN samples), or experimental (e.g., uncertainty on integrated luminosity). Some of these uncertainties affect only the normalization

TABLE II: Summary of event yields for the $\ell + b$ -tagged jet(s) + \cancel{E}_T final state in the Run IIb1 + Run IIb2 data. Events in data are compared with the expected number of ST and DT events in the $W+2$ - and $W+3$ -jets samples, in simulated samples of diboson (labeled “ WW, WZ, ZZ ” in the table), $W/Z+b\bar{b}$ or $c\bar{c}$ (“ $W/Z + b\bar{b}/c\bar{c}$ ”), W/Z +light-quark jets (“ W/Z +jets”), top quark (“ $t\bar{t}$ ” and “Single top”) production, and data-derived multijet background (“MJ”). The WH expectation is given for $M_H = 115$ GeV and includes the contribution from $ZH \rightarrow \ell b\bar{b}$ production where one of the leptons is not identified. The uncertainties include the contribution from systematic sources.

| | W+2 jets 1 b -tag | W+2 jets 2 b -tags | W+3 jets 1 b -tag | W+3 jets 2 b -tags |
|---------------------------|------------------------|-------------------------|------------------------|-------------------------|
| WW | 1030 ± 132 | 83 ± 10 | 240 ± 38 | 39 ± 5 |
| WZ | 177 ± 25 | 62 ± 7 | 44 ± 8 | 16 ± 3 |
| ZZ | 25 ± 3 | 9 ± 1 | 8 ± 2 | 3 ± 1 |
| $W/Z + b\bar{b}/c\bar{c}$ | 8468 ± 2117 | 1973 ± 461 | 2033 ± 536 | 627 ± 155 |
| W/Z +jets | 25440 ± 3643 | 1478 ± 206 | 4064 ± 648 | 455 ± 66 |
| $t\bar{t}$ | 1051 ± 214 | 717 ± 108 | 1185 ± 250 | 1119 ± 171 |
| Single top | 473 ± 78 | 216 ± 31 | 108 ± 21 | 82 ± 14 |
| MJ | 6931 ± 948 | 747 ± 102 | 1536 ± 214 | 277 ± 33 |
| WH | 19.1 ± 2.0 | 19.0 ± 1.7 | 3.9 ± 0.5 | 3.9 ± 0.9 |
| Total expectation | 43585 ± 5860 | 5285 ± 709 | 9217 ± 1386 | 2619 ± 359 |
| Observed Events | 42783 | 4881 | 8759 | 2558 |

of the signal or backgrounds, while others also affect the differential distribution of the MVA output.

Theoretical uncertainties include uncertainties on the $t\bar{t}$ and single top-quark production cross sections (10% and 12%, respectively [21, 22]), an uncertainty on the diboson production cross section (6% [23]), and an uncertainty on W +heavy-flavor production (20%, estimated from MCFM). These uncertainties affect only the normalization of these backgrounds.

Uncertainties from modeling that affect the distribution in the MVA output include uncertainties on trigger efficiency as derived from data (3–5%), lepton identification and reconstruction efficiency (5–6%), re-weighting of ALPGEN MC samples (2%), the MLM matching applied to W/Z +light-jet events ($\approx 0.5\%$), and the systematic uncertainties associated with choice of renormalization and factorization scales in ALPGEN as well as the uncertainty on the strong coupling constant (2%). Uncertainties on the ALPGEN renormalization and factorization scales are evaluated by adjusting the nominal scale for each, simultaneously, by a factor of 0.5 and 2.0.

Experimental uncertainties that affect only the normalization of the signal and SM backgrounds arise from the uncertainty on integrated luminosity (6.1%) [32]. Those that affect the MVA distribution include jet taggability (3%), b -tagging efficiency (2.5–3% per heavy quark-jet), the light-quark jet misidentification rate (10%), acceptance for jet identification (5%); jet-energy calibration and resolution (varies between 15% and 30%, depending on the process and channel). The multijet background model has a contribution from the statistical uncertainty of data after tagging (10–20%), which also covers the uncertainty in the flavor dependence of $f_{T|L}$. We do not apply additional uncertainty on the W +light jets normalization after b -tagging aside from that included in the systematic sources already mentioned.

We observe no significant excess relative to the SM expectation and proceed to set upper limits on $\sigma(WH)$ using MVA discriminants for the different channels. All bins of the MVA distribution are examined to assure sufficient Monte Carlo (MC) statistics. Those bins that do not have sufficient statistics are combined with adjacent bins until a smooth distribution that does not sacrifice sensitivity is assured. As described above, each channel is analyzed independently and the limits are then combined. We calculate all limits at 95% C.L. using the modified Frequentist CL_s approach with a Poisson log-likelihood ratio as the test statistic [33–35]. We treat systematic uncertainties as “nuisance parameters” constrained by their priors, and the best fits of these parameters are determined at each value of M_H by maximizing the likelihood. Independent fits are performed to the background-only and signal-plus-background hypotheses. All correlations are maintained among channels and between signal and background. Figure 2 shows the background-subtracted data along with the best-fit $\pm 1\sigma$ systematic uncertainties, and the signal contribution scaled by a factor of 5, for the Run IIb data. We then combine the Run IIa portion of the dataset, unchanged from the previous analysis. The log-likelihood ratios for the background-only model and the signal-plus-background model as a function of M_H are shown in Fig. 3(a). The upper limit at 95% C.L. on the cross section for $\sigma(p\bar{p} \rightarrow WH) \times \mathcal{B}(H \rightarrow b\bar{b})$ is a factor of 4.6 larger than the SM expectation for $M_H = 115$ GeV. The corresponding upper limit expected from the SM cross section and our expected sensitivity is 3.5. The same study is performed for ten other M_H values between 100 and 150 GeV. The corresponding observed and expected 95% C.L. limits relative to the SM expectation are given in Table IV and in Fig. 3(b).

As mentioned previously, we also use the MVA trained with WZ and ZZ MC events as the signal to compute the $WZ + ZZ$ cross section in the Run IIb data. We find that applying the MVAQCD (not retrained for the WZ/ZZ

TABLE III: Table of MVA discriminant input variables.

| Variable | Definition |
|--|---|
| b -ID output | summed b -tagging algorithm outputs for leading and sub-leading jets |
| m_{bb} | invariant mass formed by the pair of jets with the highest b -tagging algorithm output values |
| WH asymmetry | Mass asymmetry between W and H candidates: $(m_W - m_{bb})/(m_W + m_{bb})$ |
| Higgs decay product velocity | $-\log\left(1 - \sqrt{1 - 4\sqrt{(m_1 + m_2)/m}}\right)$ where m_1 , m_2 , and m are respectively the leading, sub-leading and di-jet invariant masses |
| $q^\ell \times \eta_\ell$ | lepton charge times pseudorapidity |
| $\Delta\eta_{max}(j, \ell)$ | the maximum $\Delta\eta$ between any jet and the lepton |
| Σ_{min} | $\frac{\Delta R(j_1, j_2) \times p_T^{j, min}}{\Sigma p_T^j}$, where $p_T^{j, min}$ corresponds to the smallest jet transverse momentum |
| $(\vec{p}_T^\ell + \vec{\cancel{E}}_T)/(\Sigma p_T)$ | vector sum of the lepton p_T and MET over their scalar sum |
| Aplanarity | $3\lambda_3/2$ where λ_3 is the smallest eigenvalue of the normalized momentum tensor $S^{\alpha\beta} = \frac{\sum_i p_i^\alpha p_i^\beta}{\sum_i p_i ^2}$, where $\alpha, \beta = 1, 2, 3$ correspond to the x, y, z momentum components and i runs over the jets and lepton |
| $q^\ell \times \eta_{j1}$ | lepton charge times the leading jet pseudorapidity |
| $m_{\ell\nu j2}$ | invariant mass of lepton, neutrino and second leading jet |
| MVAQCD | MVA QCD output after applying the MVAQCD cut (electron channel only) |
| Centrality | $\frac{\sum_i p_T^i}{\sum_i p_i }$ where i runs over the jets and lepton |
| p_T^{j2} | second leading jet p_T |

TABLE IV: Observed and expected 95% C.L. upper limits on the ratio of $\sigma(p\bar{p} \rightarrow WH) \times \mathcal{B}(H \rightarrow b\bar{b})$ to the SM expectation for each M_H value considered.

| M_H [GeV] | 100 | 105 | 110 | 115 | 120 | 125 | 130 | 135 | 140 | 145 | 150 |
|----------------------------|-----|-----|-----|-----|-----|-----|-----|-----|------|------|------|
| Exp. Limit / σ_{SM} | 2.4 | 2.6 | 3.0 | 3.5 | 4.3 | 5.4 | 7.0 | 9.6 | 13.6 | 20.4 | 33.6 |
| Obs. Limit / σ_{SM} | 2.6 | 2.9 | 4.1 | 4.6 | 5.8 | 6.8 | 8.2 | 6.3 | 10.3 | 13.3 | 23.2 |

signal) cutoff in the electron channel shifts the remaining multijet contribution to higher dijet invariant mass, making it difficult to distinguish VZ from multijet events. We therefore remove the MVAQCD requirement, and instead impose the same triangular selection as in the muon channel, increase the \cancel{E}_T requirement from 15 to 20 GeV and introduce a $H_T > 60$ GeV cutoff. Nevertheless we keep the MVAQCD output as an input variable to the final MVA.

Fig. 4 shows the dijet mass and the MVA output distributions for ST and DT data in the 2 jets channel after the fit to data with the signal+background hypothesis. Figures 5 and 6 show the corresponding background-subtracted data, along with the best-fit ± 1 standard deviation (sd), and the $WZ + ZZ$ signal expectation. Fig. 7 shows the observed LLR compared to the LLR distributions for the signal+background and background only hypotheses. Fitting to the data we measure a $WZ + ZZ$ cross section of $7.20 \pm 2.03(\text{stat.}) \pm 2.74(\text{syst.})$ pb. We determine the significance of this excess over the background only hypothesis by performing the cross section fit in background only pseudo-experiments and integrating the probability for the outcome to be as large as the observed value, as shown in Fig. 9. We determine the observed significance to be 2.2 sd above the background only hypothesis. Comparing to the predicted cross section of 4.42 pb from MCFM we find the expected significance to be 1.4 sd. Also shown in Fig. 8 is the comparison of the observation with the expected distribution of outcomes in the signal+background hypothesis.

In conclusion, a search for WH production in $\ell + \cancel{E}_T + 2$ or 3-jets final states with 8.5 fb^{-1} of integrated luminosity

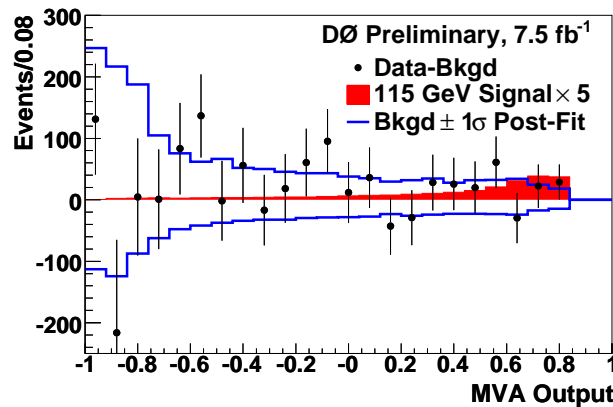


FIG. 2: Distribution in the output of the MVA discriminant for $M_H = 115$ GeV, for the difference between data and background expectation, combined for all channels (both e and μ , ST and DT, and 2-jet and 3-jet), for the 7.5 fb^{-1} Run IIB1 + Run IIB2 dataset, shown with statistical uncertainties. The solid lines represent the total systematic uncertainty after constraining with data (“Post-Fit” in the legend). The darker shaded region represents the SM Higgs signal expectation scaled up by a factor of 5.

at the D0 detector, using of single and double b -tagged jets has been performed. The results are in agreement with the expected background, and we set upper limits on $\sigma(pp \rightarrow WH) \times \mathcal{B}(H \rightarrow b\bar{b})$ relative to the SM expectations $\sigma(\text{SM})$ for Higgs masses between 100 and 150 GeV, as summarized in Table IV and shown in Fig. 3b. For $M_H = 115$ GeV, the ratio of the observed (expected) 95% C.L. limit/(SM) is 4.6 (3.5). We also compute the $WZ + ZZ$ cross section using a dedicated MVA output distribution as the template, and find a $WZ + ZZ$ cross section of $7.20 \pm 2.03(\text{stat.}) \pm 2.74(\text{syst.})$ pb, corresponding to a significance of 2.2 sd.

We thank the staffs at Fermilab and collaborating institutions, and acknowledge support from the DOE and NSF (USA); CEA and CNRS/IN2P3 (France); FASI, Rosatom and RFBR (Russia); CNPq, FAPERJ, FAPESP and FUNDUNESP (Brazil); DAE and DST (India); Colciencias (Colombia); CONACyT (Mexico); KRF and KOSEF (Korea); CONICET and UBACyT (Argentina); FOM (The Netherlands); STFC and the Royal Society (United Kingdom); MSMT and GACR (Czech Republic); CRC Program and NSERC (Canada); BMBF and DFG (Germany); SFI (Ireland); The Swedish Research Council (Sweden); and CAS and CNSF (China).

-
- [1] ALEPH, DELPHI, L3, and OPAL Collaborations, The LEP Working Group for Higgs Boson Searches, Phys. Lett. B **565**, 61 (2003).
- [2] LEP Electroweak Working Group, <http://lepewwg.web.cern.ch/LEPEWWG/>
- [3] The CDF, D0 Collaborations, the TEVNPWWG Working Group, arXiv:1103.3233 [hep-ex] ; CDF and D0 Collaborations, T. Aaltonen *et al.*, Phys. Rev. Lett. **104**, 061802 (2010).
- [4] D0 Collaboration, V.M. Abazov *et al.*, Phys. Rev. Lett. **94**, 091802 (2005).
- [5] D0 Collaboration, V.M. Abazov *et al.*, Phys. Lett. B **663**, 26 (2008).
- [6] D0 Collaboration, V.M. Abazov *et al.*, Phys. Rev. Lett. **102**, 051803 (2009).
- [7] D0 Collaboration, V.M. Abazov *et al.*, Phys. Lett. B **698**, 6 (2011).
- [8] CDF Collaboration, T. Aaltonen *et al.*, Phys. Rev. Lett. **103**, 101802 (2009).
- [9] DØ Collaboration, V. Abazov *et al.*, Nucl. Instrum. Meth., Res. A **565**, 463 (2006).
- [10] Pseudorapidity $\eta = -\ln[\tan \frac{\theta}{2}]$, where θ is the polar angle as measured from the beam axis; ϕ is the azimuthal angle. The separation between two objects in η, ϕ space is $\Delta\mathcal{R} = \sqrt{(\Delta\eta)^2 + (\Delta\phi)^2}$.
- [11] S. Abachi, *et al.*, Nucl. Instrum. Methods Phys. Res. A **338**, 185 (1994).
- [12] R. Angstadt *et al.*, Nucl. Instrum. Methods in Phys. Res. Sect. A **622**, 298 (2010).
- [13] M. Abolins *et al.*, Nucl. Instrum. and Methods A **584**, 75 (2008).
- [14] H. L. Lai *et al.*, Phys.Rev. D **55**, 1280 (1997), <http://hep.pa.msu.edu/people/wkt/cteq6/cteq6pdf.html>
J. Pumplin *et al.*, JHEP07(2002)012, arXiv:hep-ph/0201195v3.
- [15] T. Sjostrand, P. Eden, C. Friberg, L. Lonnblad, G. Miu, S. Mrenna and E. Norrbin, Comput. Phys. Commun. **135**, (2001) 238, versions 6.319, 6.323 and 6.409.
- [16] M. Mangano *et al.*, ALPGEN, hep-ph/0206293, JHEP07 (2003) 001, version 2.05, <http://mlm.web.cern.ch/mlm/alpgen>
- [17] A. Pukhov *et al.*, COMPHEP, hep-ph/9908288 (1999).

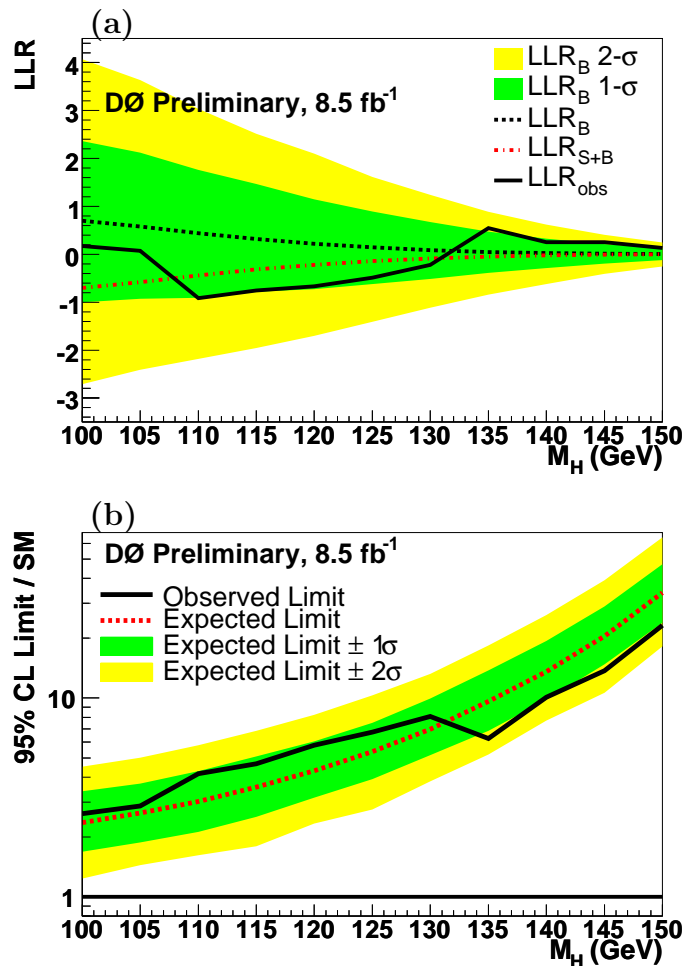


FIG. 3: Results obtained with the combined Run IIA and Run IIB data: (a) Log-likelihood ratio for the background-only model (LLR_B , with 1σ and 2σ uncertainty bands), signal+background model (LLR_{S+B}) and observation in data (LLR_{OBS}) vs. M_H . (b) 95% C.L. cross section upper limit (and corresponding expected limit) on $\sigma(p\bar{p} \rightarrow WH) \times \mathcal{B}(H \rightarrow b\bar{b})$ relative to the SM expectation vs. M_H .

- [18] R. Brun and F. Carminati, CERN Program library Long Writeup, Report W5013 (1993).
- [19] J. Baglio and A. Djouadi, arXiv:1003.4266v2 [hep-ph].
- [20] A. D. Martin, W. J. Stirling, R. S. Thorne and G. Watt, Eur. Phys. J. C **63**, 189 (2009) [arXiv:0901.0002 [hep-ph]].
- [21] N. Kidonakis *et al.*, Phys. Rev. D **78**, 074005 (2008).
- [22] N. Kidonakis, Phys. Rev. D **74**, 114012 (2006).
- [23] J. Campbell and K. Ellis, MCFM, <http://mcfm.fnal.gov/>
- [24] R. Hamberg, W.L. van Neerven, and W.B. Kilgore, Nucl. Phys. B **359**, 343 (1991); B **644**, 403 (2002).
- [25] A.D. Martin, R.G. Roberts, W.J. Stirling, and R.S. Thorne, Phys. Lett. B **604**, 61 (2004).
- [26] J. Hegeman, J. Phys. Conf. Ser. **160**, 012024 (2009).
- [27] V. Abazov *et al.* (DØ Collaboration), Phys. Rev. D **76**, 092007 (2007).
- [28] G. Blazey *et al.*, in *Proceedings of the workshop "QCD and Weak Boson Physics in Run II"* edited by U. Baur, R.K. Ellis, and D. Zeppenfeld, Batavia (2000), p. 47. arXiv:hep-ex/0005012 (2000).
- [29] J. Alwall *et al.*, Eur. Phys. C **53**, 473 (2008).
- [30] A. Hoecker, P. Speckmayer, J. Stelzer, J. Therhaag, E. von Toerne, and H. Voss, "TMVA: Toolkit for Multivariate Data Analysis," PoS A CAT 040 (2007) [physics/0703039].
- [31] V.M. Abazov *et al.* (DØ Collaboration), Nucl. Instrum. Methods Phys. Res. A **620**, 490 (2010).
- [32] T. Andeen, *et al.*, FERMILAB-TM-2365, April 2007.
- [33] T. Junk, Nucl. Instrum. Meth. A **434**, p. 435-443, 1999.
- [34] A. Read, J. Phys. G **28**, 2693 (2002).
- [35] W. Fisher, FERMILAB-TM-2386-E (2007).

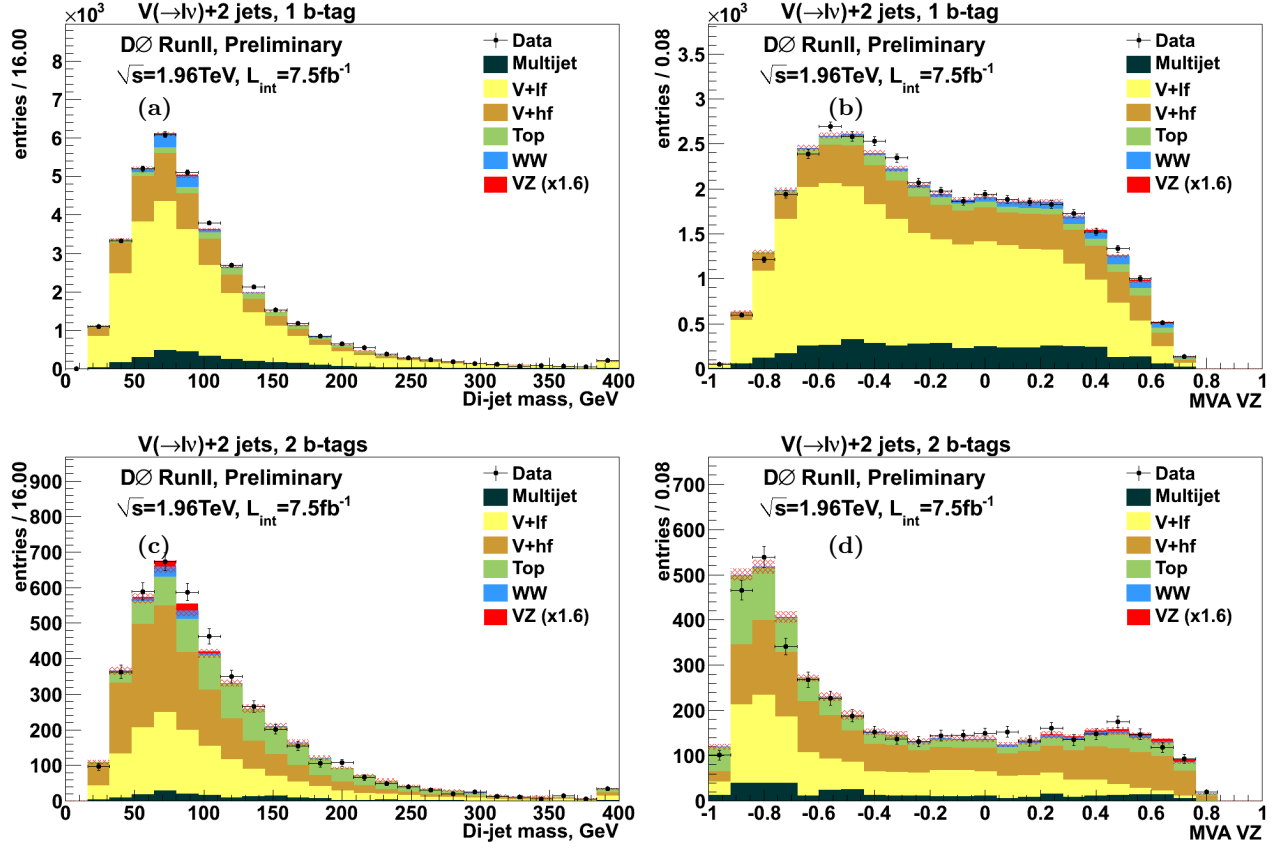


FIG. 4: Distributions for $W+2$ -jets ST (a,b) and DT (c,d) data of the dijet invariant mass and the output of the $WZ + ZZ$ (collectively called VZ) MVA discriminant after the fit to the data under the signal+background hypothesis. The dibosons signal distributions (filled red histogram) are scaled to their measured cross-sections. The hatched area represents the statistical error on the total background.

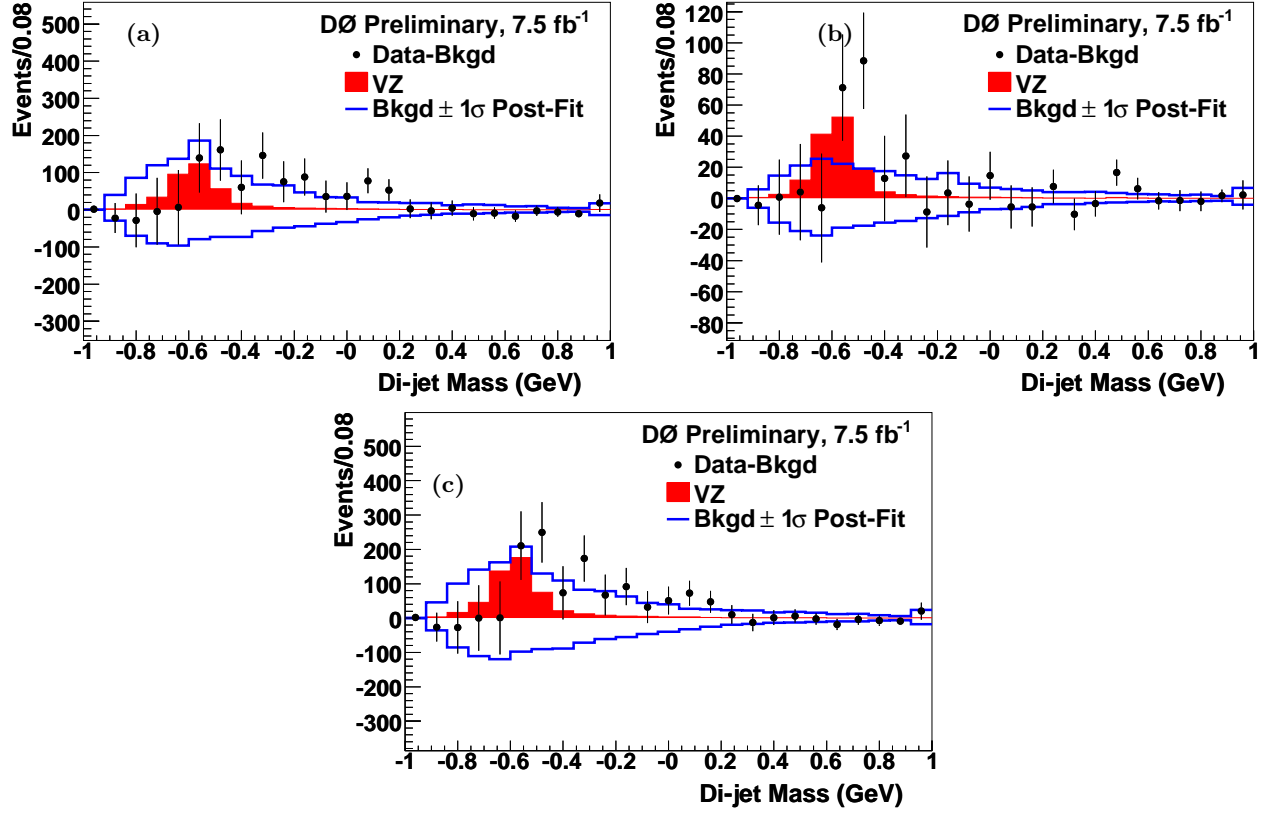


FIG. 5: Difference in the dijet mass distributions (in the range [0-400] GeV normalized to [-1,1]) between data and background expectation after the fit to the data under the signal+background hypothesis. They are combined for ST (a), DT (b) and all (c) channels (both e and μ , ST and DT, and 2-jet and 3-jet), for the 7.5 fb^{-1} Run IIb1 + Run IIb2 dataset, shown with statistical uncertainties. The solid lines represent the total systematic uncertainty after constraining with data (“Post-Fit” in the legend). The darker shaded region represents the $WZ + ZZ$ signal scaled to the the fitted cross section.

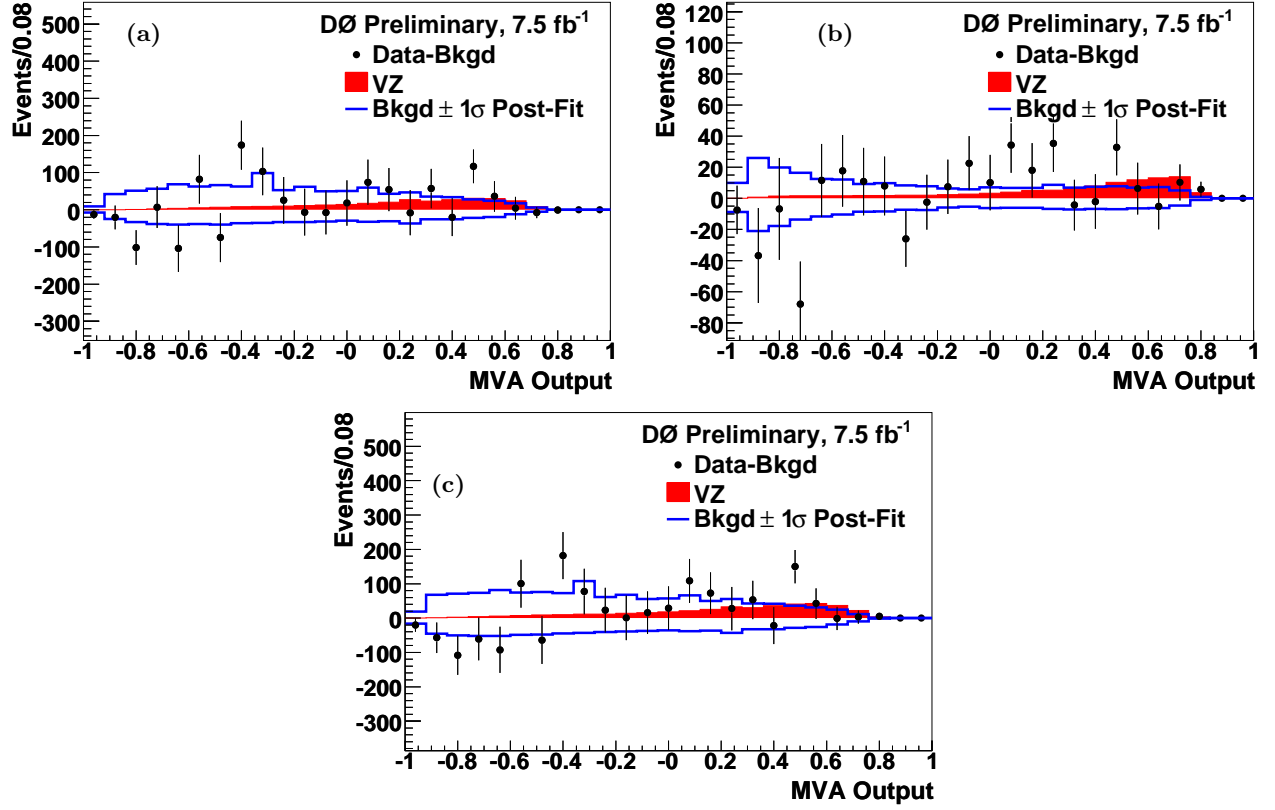


FIG. 6: Difference in the final MVA distributions between data and background expectation after the fit to the data under the signal+background hypothesis. They are combined for ST (a), DT (b) and all (c) channels (both e and μ , ST and DT, and 2-jet and 3-jet), for the 7.5 fb^{-1} Run IIb1 + Run IIb2 dataset, shown with statistical uncertainties. The solid lines represent the total systematic uncertainty after constraining with data (“Post-Fit” in the legend). The darker shaded region represents the $WZ + ZZ$ signal scaled to the fitted cross section.

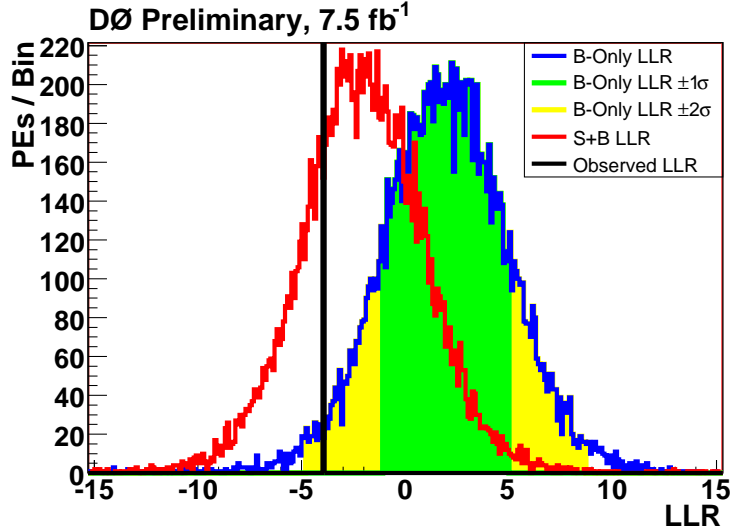


FIG. 7: Observed Log-likelihood ratio (LLR) compared to the LLR distributions for the signal+background and background only hypotheses for the $WZ + ZZ$ cross section measurement, with all channels combined. The MVA output is used as the test variable.

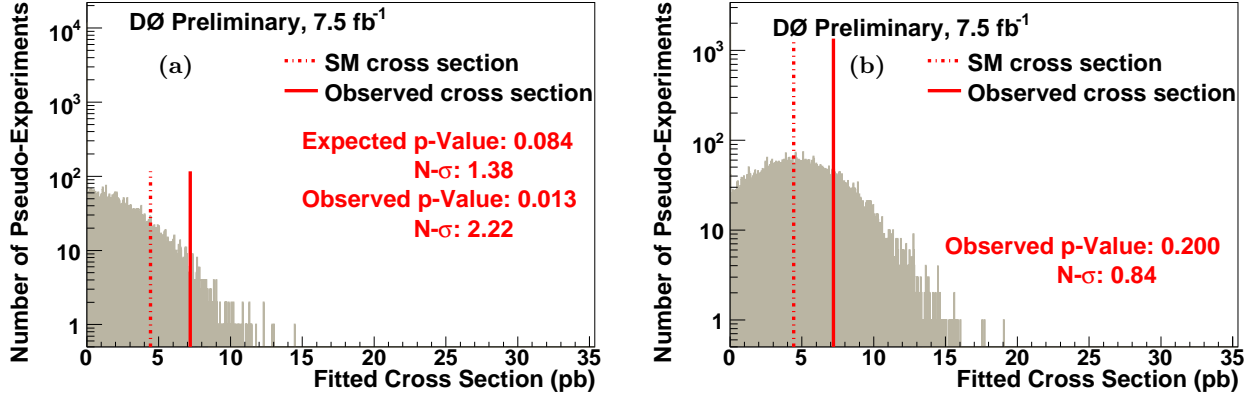


FIG. 8: (a) Expected and observed sensitivity to $WZ + ZZ$ production, computed with null-hypothesis pseudoexperiments (shown in grey), (b) deviation of fitted cross section from the SM expectation, computed with S+B-hypothesis pseudoexperiments (shown in grey), for all Run IIb channels combined. The MVA output is used as the test variable.